Synthesis and Isolation of {110}-Faceted Gold Bipyramids and Rhombic Dodecahedra

ARTICLE *in* JOURNAL OF THE AMERICAN CHEMICAL SOCIETY · MARCH 2011

Impact Factor: 12.11 · DOI: 10.1021/ja201826r · Source: PubMed

3-1-2011

Synthesis and Isolation of {110}-Faceted Gold Bipyramids and Rhombic Dodecahedra

Michelle L. Personick
Northwestern University

Mark R. Langille
Northwestern University, MarkLangille2013@u.northwestern.edu

Jian Zhang
University of Nebraska-Lincoln, jzhang3@unl.edu

Nadine Harris
Northwestern University

George C. Schatz
Northwestern University

See next page for additional authors

Published in *Journal of the American Chemical Society* 133:16 (2011), pp. 6170–6173; doi: 10.1021/ja201826r

Published online March 31, 2011.

Synthesis and Isolation of {110}-Faceted Gold Bipyramids and Rhombic Dodecahedra

Michelle L. Personick, Mark R. Langille, Jian Zhang, Nadine Harris, George C. Schatz, and Chad A. Mirkin

Department of Chemistry and International Institute for Nanotechnology, Northwestern University, 2145 Sheridan Road, Evanston, Illinois 60208, United States

Corresponding author — C. A. Mirkin, chadnano@northwestern.edu

Abstract

Two {110}-faceted gold nanostructures—rhombic dodecahedra and obtuse triangular bipyramids—have been synthesized via a Ag-assisted, seed-mediated growth method. The combination of a Cl^--containing surfactant with a low concentration of Ag^+ plays a role in the stabilization of the {110} facets. To the best of our knowledge, this is the first reported synthesis of a {110}-faceted bipyramid structure.

The unique physical and chemical properties of nanoscale materials are dependent on their composition, size, and shape. In the case of noble metal nanostructures, the ability to selectively synthesize particles of a particular architecture enables rational control over their plasmonic, catalytic, electrical, and magnetic properties.[1] For example, the crystallographic facets exposed on the surface of a transition metal nanoparticle (i.e., shape) can significantly affect its catalytic properties with respect to both activity and selectivity.[1d] In addition to dictating chemical properties, control of the architectural parameters of a noble metal nanoparticle allows the surface plasmon resonance (SPR) of that particle to be easily tuned to a desired wavelength.[2] Among the noble metals, Au nanoparticles are especially appealing due to a combination of properties, including intense SPRs,[3] potential for catalytic applications,[4] and tailorable surface-enhancing spectroscopic effects.[5] One of the most effective methods for controlling the shape and, consequently, the physical and chemical properties of Au nanostructures is by a thermal, seed-mediated synthetic method. Although a variety of well-defined shapes can be obtained via this approach by varying factors such as temperature, surfactant, and reducing agent and by introducing shape-directing additives such as underpotentially deposited metals,[6] the literature is dominated by morphologies such as cubes, octahedra, rods, and prisms, which are primarily defined by {111} and {100} facets.[6e, 7] While a few Au nanostructures with high-index facets—tetrahexahedra, tris-octahedra, and concave cubes—have been recently reported,[8] the selective stabilization of {110} facets has proven to be challenging. Herein, we report the first method for synthesizing {110}-faceted bipyramids, which form concomitantly with rhombic dodecahedra. Importantly, the novel bipyramids can be separated from the rhombic dodecahedra via filtration to produce high-quality, monodisperse samples of each of the {110}-faceted nanostructures.

For Au, which is a face-centered cubic (FCC) metal, the surface energies of the low-index crystallographic facets usually increase in the order $\gamma_{\{111\}} < \gamma_{\{100\}} < \gamma_{\{110\}}$.[9] Because {110} facets have the highest surface energy among the low-index facets, they generally provide the most favorable surface for Au atom deposition. This typically results in the disappearance of {110} facets as a particle grows and makes {110}-faceted nanoparticles difficult to synthesize.[6d, 8e] As a result, most syntheses for {110}-faced nanoparticles require high temperatures or complicated synthetic procedures and often result in particles with poorly defined facets or high size dispersity.[6d, 10] Below, we describe the facile synthesis and isolation of two high-quality {110}-faceted Au nanoparticle morphologies: rhombic dodecahedra and obtuse triangular bipyramids. Due to the unique shape of the {110}-faceted bipyramids, they may have potential use for novel applications, particularly in plasmonics.

The rhombic dodecahedra and bipyramids were synthesized using a seed-mediated, Ag-assisted growth procedure. Briefly, a solution of 7 nm Au seed particles was prepared by the rapid reduction of $HAuCl_4$ by $NaBH_4$ in the presence of cetyltrimethylammonium chloride (CTAC). A growth solution was prepared by sequentially adding 0.5 mL of 10 mM $HAuCl_4$, 0.01 mL of 10 mM $AgNO_3$, 0.2 mL of 1.0 M HCl, and 0.1 mL of 100 mM ascorbic acid to a 10 mL aqueous solution of 0.04 M CTAC and 0.6 mL of 1.0 M NaCl. The reaction was initiated by the addition of 0.1 μL of the Au seed particles (prepared by serial dilution) to the growth solution and mixed gently. The reaction solution was allowed to sit undisturbed overnight (Supporting Information).

Characterization of the products by SEM indicates that the reaction yields two different particle morphologies: smaller rhombic dodecahedra (RD) and larger triangular bipyramids (BPs) (Figure 1A). Both particles have well-defined surfaces with sharp edges and corners. While there is a large size discrepancy between the smaller RD (edge length of 31 ± 5 nm) and the larger BPs (edge length of 270 ± 26 nm), the size dispersity between particles of the same morphology is relatively low. Typical diffraction patterns obtained from individual RD (Figure 1B) and BPs (Figure 1C) with the electron beam perpendicular to the substrate are characteristic of the [110] zone axis of FCC Au, indicating that both particles lie with a {110} facet flat against the substrate (Figure S1). Consistent with the TEM data, high-magnification SEM images of the RD show that all of the 12 rhombic faces are identical (Figure 1D), as are the six triangular

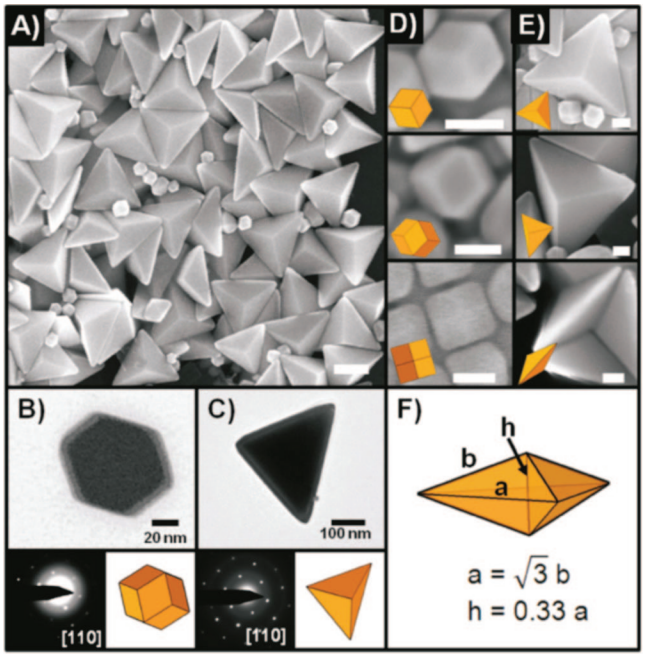

Figure 1. (A) Low-magnification SEM image of the reaction product containing both rhombic dodecahedra and bipyramids (scale bar: 200 nm). TEM image, diffraction pattern, and model of (B) a rhombic dodecahedron and (C) a bipyramid. High-magnification SEM images and models of (D) the rhombic dodecahedra and (E) the bipyramids in various orientations (scale bars: 50 nm). (F) Geometric model of a bipyramid.

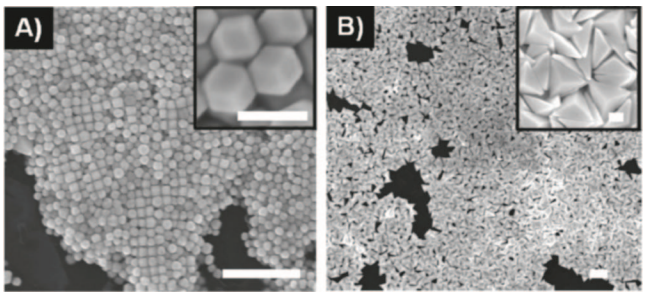

Figure 2. Low-magnification SEM image of separated rhombic dodecahedra (A) and bipyramids (B). Scale bars: 500 nm (low-magnification images), 100 nm (inset).

facets of the BPs (Figure 1E), leading to the conclusion that both particles are bound exclusively by {110} facets.

Although the RD and the BPs share the same surface facets, they have strikingly different morphologies, which we propose arises from differences in particle crystallinity. The shape of the RD (Figure 1B,1D) is consistent with single-crystal particles bound by 12 identical {110} facets, while the shape of the BPs (Figure 1C,1E,S2) is consistent with two triangular pyramids joined by a (111) twin plane(s). Indeed, high-resolution TEM (HR-TEM) confirms the presence of a twin defect in the BPs (Figure S3). Particles having a {110}-faceted bipyramid structure have not previously been described. It should be noted that, unlike {100}-faceted right triangular bipyramids previously reported in literature,[11] these {110}-faceted bipyramids are significantly more planar structures, having an angle of 120° between their facets at the 3-fold vertices, compared to 90° for right bipyramids. The ratio of the edge length to the

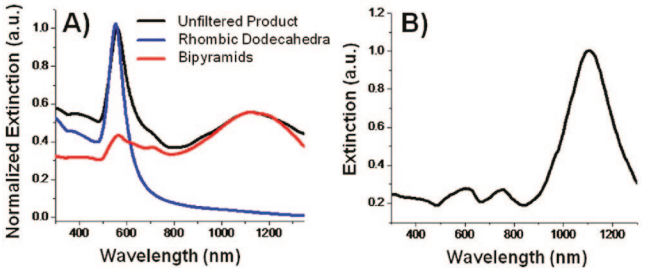

Figure 3. (A) UV−vis spectrum of separated RD (blue) and BPs (red) compared to the mixed solution (black). (B) DDA orientationally averaged calculated extinction spectrum for a BP with an edge length of 270 nm.

height (herein defined as aspect ratio) of the {110}-faceted bipyramid is approximately 3:1 (Figure 1F).

Due to the large size difference between the two products, they can be easily separated by filtration (Supporting Information) to yield high-purity samples of monodisperse rhombic dodecahedra (Figure 2A) and bipyramids (Figure 2B). The effectiveness of the separation was examined by UV−visible (UV−vis) spectroscopy. The UV−vis spectrum of the product solution before separation shows two major peaks: one resonance in the visible region (~560 nm) and one in the near-infrared region (NIR) (~1130 nm) (Figure 3A). After separation, the solution of pure RD displays only a single resonance in the visible region, while the major extinction peak from the solution of pure BPs is in the NIR. Due to the high aspect ratio of the BPs, they are expected to have a significantly red-shifted resonance from the near-spherical RD.[1a] The UV−vis spectrum of the BPs also suggests the presence of higher order resonances at shorter wavelengths (one at 565 nm and another at 710 nm) consistent with other highly anisotropic planar gold particles, such as triangular nanoprisms.[7a] Indeed, theoretically calculated optical properties of the BPs using the discrete dipole approximation (DDA) method[12] (Supporting Information) confirm the presence of three major SPRs: a dipole mode at ~1110 nm, a higher order quadrupole mode at ~750 nm, and an octopole mode at ~600 nm (Figure 3B).

We propose that the RD and BP morphologies arise from the deposition of Au onto single-crystal and planar-twinned seeds, respectively. Using HR-TEM, we determined that the 7 nm diameter CTAC-protected seed particles used to initiate the reaction are, indeed, a mixture of single crystalline and planar-twinned structures (Figure S4). Growth from these seed particles was monitored by UV−vis (Figure S5). As early as 15 min into the reaction, a small absorbance peak and shoulder were detected, which are attributed to the RD and the BPs, respectively. As the reaction progresses, the RD peak grows in intensity over time and red-shifts only slightly, while the peak for the BPs has a much more pronounced shift, moving into the NIR. The concurrent evolution of both RD and BP from the growth solution suggests that the twin structure of the seed particles dictates the twin structure of the final product. In line with this hypothesis, if single-crystal seeds are exclusively used to nucleate the reaction, only RD are observed in the reaction product (Figure S6). This suggests that it is the planar-twinned seeds that are responsible for the generation of BPs and that the self-nucleation of twinned seeds is not a large contributing factor to their presence.

The significant size discrepancy between the large BPs and the small RD can be understood based on the preferred reduction of Au onto planar-twinned seeds as compared to single-crystal seeds. It is generally believed that metal reduction is more favorable at twin defects due to the presence of re-entrant grooves.[13] However, it is interesting that, in this particular synthesis, the twinned particles grow to sizes many times that of their single-crystal counterparts. Similar to previously published seed-mediated syntheses, the size of the product can be controlled by adjusting the amount of seed particles added, with more seed particles providing more nucleation sites and thus leading to smaller nanoparticles. Interestingly, as the size of the products decreases from the addition of more seeds, the size difference between the BPs and the RD also decreases, as confirmed by SEM and UV−vis (Figure S7). This suggests that when the Au^{3+}/seed ratio is low, there is little deposition preference for either of the two types of seed particles. However, as the Au^{3+}/seed ratio is increased, the deposition favors the twinned particles over the single-crystal particles. This is likely due to the decreasing reactivity of the particles as they grow in size. At small sizes, the reactivities of both particles are comparable, while at large sizes, the single-crystal RD become significantly less reactive than the twinned BPs due to the presence of the twin defect in the BPs, allowing the BPs to grow much larger in size.

Both the twinned BPs and single-crystalline RD products are unusual in that they are both enclosed by {110} facets. Of the low-index facets, {110} facets are the most open and have the highest surface energy, while {111} facets are the most thermodynamically stable.[9] In general, it would be expected that Au would deposit onto the higher energy {110} surfaces and thus the lower energy {111} facets would be retained in the final structure if the reaction is thermodynamically controlled. However, when a small amount of Ag^+ is introduced to the reaction, it is believed that up to a monolayer of Ag can be deposited onto the growing Au particle surface through the phenomenon of underpotential deposition (UPD) and can play a major role in subsequent particle growth by inhibiting the reduction of Au onto that surface.[6c, 14] Ag will preferentially be reduced onto the highest energy facets of a Au particle, stabilizing those facets, and retaining them in the final product. In previously reported UPD seed-mediated syntheses,[6a-6c, 8a-8c] Ag^+/Au^{3+} ratios as high as 1:5 are used to generate morphologies such as {730}-faceted tetrahexahedra[8a] and {711}-faceted penta-twinned bipyramids,[6c,15] synthesized in a bromide-containing surfactant such as cetyltrimethylammonium bromide (CTAB), or {720}-faceted concave cubes synthesized in CTAC.[8b] Here, we have demonstrated that the stabilization of the higher energy low-index {110} facet can be achieved by simply decreasing the Ag^+/Au^{3+} ratio to 1:50, although the use of a Cl^--containing surfactant (CTAC) appears to be essential for the generation of {110}-faced RD and BPs. When the analogous Br^--containing surfactant (CTAB) is used, particles enclosed entirely by {110} facets are not observed, but rather, a variety of nonuniform particles with ill-defined facets are formed (Figure S8). This may be due to the stronger binding of Br^- than Cl^- to Au surfaces.[16] We hypothesize that the low binding affinity of Cl^- for Au surfaces allows the effects of Ag UPD to predominate over surfactant effects—even at a low Ag^+ concentration—in this CTAC-based, seed-mediated growth method. However, our investigations into the synergistic effects of Ag^+ and Cl^- on Au nanoparticle growth are still ongoing.

In conclusion, high-purity samples of {110}-faceted rhombic dodecahedra and their novel planar-twinned counterpart, {110}-faceted bipyramids, have been prepared by an Ag-assisted, seed-mediated synthesis. These structures arise from the deposition of Au onto either single-crystal or planar-twinned seed particles to yield the RD and BPs, respectively. Using a low Ag^+/Au^{3+} ratio (1:50) in combination with a Cl^--containing surfactant leads to the stabilization of a higher energy low-index facet, which has not been previously demonstrated. Filtration techniques can be used to isolate high-purity samples of both particle types. The RD have possible utility for catalysis[4] as well as for SERS,[5] and the {110}-faceted bipyramids may be useful for many potential applications due to their NIR resonance. These bipyramids are highly stable and are expected to be more resistant to oxidative etching than other structures with NIR resonances, such as Au triangular nanoprisms, and therefore have potential use in applications.

Acknowledgments — This work was supported by the MRSEC program of the National Science Foundation at the Material Research Center of Northwestern University. This material is based upon work supported as part of the Non-Equilibrium Energy Research Center (NERC), an Energy Frontier Research Center funded by the U.S. Department of Energy, Office of Science, Office of Basic Energy Sciences under Award Number DE-SC0000989. The microscopy work was performed in the EPIC facility of NUANCE Center at Northwestern University and the authors thank Dr. Shuyou Li for assistance with the HR-TEM work. NUANCE Center is supported by NSF-NSEC, NSF-MRSEC, Keck Foundation, the State of Illinois, and Northwestern University. M.P. gratefully acknowledges support from the Department of Defense (DoD) through the National Defense Science & Engineering Graduate Fellowship (NDSEG) Program. C.A.M is grateful for an NSSEF Fellowship from the DoD.

Supporting Information, including experimental details; further discussion of DDA results; electron diffraction; additional SEM, TEM, and models of BPs; HR-TEM of twin plane; HR-TEM of seeds; UV−vis spectra monitoring particle growth; SEM of RD made with single-crystal seeds; UV−vis and SEM of size-controlled products; and SEM of particles synthesized in CTAB is presented following the **References**.

References

1. (a) Jin, R.; Cao, Y.; Mirkin, C. A.; Kelly, K. L.; Schatz, G. C.; Zheng, J. G. *Science* 2001, 294, 1901 (b) Somorjai, G. A.; Frei, H.; Park, J. Y. *J. Am. Chem. Soc.* 2009, 131, 16589 (c) Hurst, S. J.; Payne, E. K.; Qin, L.; Mirkin, C. A. *Angew. Chem., Int. Ed.* 2006, 45, 2672 (d) Xia, Y.; Xiong, Y.; Lim, B.; Skrabalak, S. E. *Angew. Chem., Int. Ed.* 2009, 48, 60 (e) Tao, A. R.; Habas, S.; Yang, P. *Small* 2008, 4, 310 (f) Millstone, J. E.; Hurst, S. J.; Metraux, G. S.; Cutler, J. I.; Mirkin, C. A. *Small* 2009, 5, 646
2. Jin, R.; Cao, Y.; Hao, E.; Metraux, G. S.; Schatz, G. C.; Mirkin, C. A. *Nature* 2003, 425, 487
3. Jain, P. K.; Lee, K. S.; El-Sayed, I. H.; El-Sayed, M. A. *J. Phys. Chem. B* 2006, 110, 7238

4. Hashmi, A. S. K.; Hutchings, G. J. *Angew. Chem., Int. Ed.* 2006, 45, 7896

5. Haynes, C. L.; McFarland, A. D.; Van Duyne, R. P. *Anal. Chem.* 2005, 77, 338

6. (a) Jana, N. R.; Gearheart, L.; Murphy, C. J. *J. Phys. Chem. B* 2001, 105, 4065 (b) Nikoobakht, B.; El-Sayed, M. A. *Chem. Mater.* 2003, 15, 1957 (c) Liu, M.; Guyot-Sionnest, P. *J. Phys. Chem. B* 2005, 109, 22192 (d) Niu, W.; Zheng, S.; Wang, D.; Liu, X.; Li, H.; Han, S.; Chen, J.; Tang, Z.; Xu, G. *J. Am. Chem. Soc.* 2009, 131, 697 (e) Sau, T. K.; Murphy, C. J. *J. Am. Chem. Soc.* 2004, 126, 8648

7. (a) Millstone, J. E.; Park, S.; Shuford, K. L.; Qin, L.; Schatz, G. C.; Mirkin, C. A. *J. Am. Chem. Soc.* 2005, 127, 5312 (b) Kim, D.; Heo, J.; Kim, M.; Lee, Y. W.; Han, S. W. *Chem. Phys. Lett.* 2009, 468, 245 (c) Johnson, C. J.; Dujardin, E.; Davis, S. A.; Murphy, C. J.; Mann, S. *J. Mater. Chem.* 2002, 12, 1765 (d) Huang, X.; Qi, X.; Huang, Y.; Li, S.; Xue, C.; Gan, C. L.; Boey, F.; Zhang, H. *ACS Nano* 2010, 4, 6196

8. (a) Ming, T.; Feng, W.; Tang, Q.; Wang, F.; Sun, L.; Wang, J.; Yan, C. *J. Am. Chem. Soc.* 2009, 131, 16350 (b) Zhang, J.; Langille, M. R.; Personick, M. L.; Zhang, K.; Li, S.; Mirkin, C. A. *J. Am. Chem. Soc.* 2010, 132, 14012 (c) Li, J.; Wang, L.; Liu, L.; Guo, L.; Han, X.; Zhang, Z. *Chem. Commun.* 2010, 46, 5109 (d) Yu, Y.; Zhang, Q.; Lu, X.; Lee, J. Y. *J. Phys. Chem. C* 2010, 114, 11119 (e) Wu, H.-L.; Kuo, C.-H.; Huang, M. H. *Langmuir* 2010, 26, 12307 (f) Carbo-Argibay, E.; Rodriguez-Gonzalez, B.; Gomez-Grana, S.; Guerrero-Martinez, A.; Pastoriza-Santos, I.; Perez-Juste, J.; Liz-Marzan, L. M. *Angew. Chem., Int. Ed.* 2010, 49, 9397 (g) Katz-Boon, H.; Rossouw, C. J.; Weyland, M.; Funston, A. M.; Mulvaney, P.; Etheridge, *J. Nano Lett.* 2011, 11, 273

9. Wang, Z. L. *J. Phys. Chem. B* 2000, 104, 1153

10. Jeong, G. H.; Kim, M.; Lee, Y. W.; Choi, W.; Oh, W. T.; Park, Q.-H.; Han, S. W. *J. Am. Chem. Soc.* 2009, 131, 1672

11. (a) Wiley, B. J.; Xiong, Y.; Li, Z.-Y.; Yin, Y.; Xia, Y. *Nano Lett.* 2006, 6, 765 (b) Zhang, J.; Li, S.; Wu, J.; Schatz, G. C.; Mirkin, C. A. *Angew. Chem., Int. Ed.* 2009, 48, 7787

12. (a) Draine, B. T.; Flatau, P. J. *J. Opt. Soc. Am. A* 1994, 11, 1491 (b) Draine, B. T.; Flatau, P. J.*User Guide to the Discrete Dipole Approximation Code DDSCAT 7.1.* http://arxiv.org/abs/1002.1505v1 (2010) .

13. (a) Jagannathan, R.; Mehta, R. V.; Timmons, J. A.; Black, D. L. *Phys. Rev. B* 1993, 48, 13261 (b) Lofton, C.; Sigmund, W. *Adv. Funct. Mater.* 2005, 15, 1197

14. (a) Sanchez, C. G.; Del Popolo, M. G.; Leiva, E. P. M. *Surf. Sci.* 1999, 421, 59 (b) Rojas, M. I.; Sanchez, C. G.; Del Popolo, M. G.; Leiva, E. P. M. *Surf. Sci.* 2000, 453, 225 (c) Leiva, E. *Electrochim. Acta* 1996, 41, 2185 (d) Hsu, S. J.; Su, P. Y. S.; Jian, L. Y.; Chang, A. H. H.; Lin, I. J. B. *Inorg. Chem.* 2010, 49, 4149

15. Kou, X.; Ni, W.; Tsung, C.-K.; Chan, K.; Lin, H.-Q.; Stucky, G. D.; Wang, J. *Small* 2007, 3, 2103

16. Ha, T. H.; Koo, H.-J.; Chung, B. H. *J. Phys. Chem. C* 2007, 111, 1123

Supporting Information for

Synthesis of {110}-Faceted Gold Bipyramids and Rhombic Dodecahedra

Michelle L. Personick, Mark R. Langille, Jian Zhang, Nadine Harris, George C. Schatz, and Chad A. Mirkin*

Department of Chemistry and International Institute for Nanotechnology, Northwestern University, 2145 Sheridan Road, Evanston, IL 60208

E-mail: chadnano@northwestern.edu

Experimental Details

Chemicals. Gold (III) chloride trihydrate ($HAuCl_4 \cdot 3H_2O$, 99.9+%), silver nitrate ($AgNO_3$, 99.9999%), sodium borohydrate ($NaBH_4$, 99.99%), sodium chloride (NaCl, 99.999%), L-ascorbic acid (AA, 99+%), and cetyltrimethylammonium chloride (CTAC, 25 wt.% in H_2O) were purchased from Aldrich and used without further purification. Hydrochloric acid (HCl, 1 mol/L volumetric solution) was purchased from Fluka and used without further purification.

Synthesis of Au Seeds. Au seeds were prepared by quickly injecting 0.60 mL of ice-cold, freshly prepared $NaBH_4$ (10 mM) into a rapidly stirring solution containing 0.25 mL of $HAuCl_4$ (10 mM) and 10.00 mL of CTAC (100 mM). The seed solution was stirred for 1 minute and then left undisturbed for 2 hours.

Synthesis of Single Crystal Seeds. Single crystal seeds were prepared according to a previously published procedure.[1]

Synthesis of Rhombic Dodecahedra and Bipyramids. A growth solution was prepared by consecutively adding 0.50 mL of $HAuCl_4$ (10 mM), 0.01 mL of $AgNO_3$ (10 mM), 0.20 mL of HCl (1.0 M), then 0.10 mL of ascorbic acid (100 mM) into 10.00 mL of 0.04 M CTAC. The seed particles were serially diluted in 0.1 M CTAC to generate a solution which was 1/1000 the concentration of the original seed solution. Particle growth was initiated by adding 0.1 mL of the diluted seeds to the growth solution. The reaction was swirled immediately after the addition of the seeds and then left undisturbed on the bench top until the reaction was complete. Bipyramids were isolated from rhombic dodecahedra via vacuum filtration with a 0.1 μm pore size filter (Whatman Anodisc 47, 0.1 μm pore, 47 mm). Alternatively, rhombic dodecahedra can also be isolated from the combined reaction mixture via syringe filtration using a syringe-driven filter with pore size ≤ 0.2 μm (PALL Life Sciences Acrodisk LC 25 mm syringe filter, 0.2 μm pore PVDF membrane).

Characterization. Scanning electron microscopy (SEM) images were obtained using a Hitachi S-4800-II cFEG SEM. Transmission electron microscopy (TEM) images and electron diffraction patterns were obtained using a Hitachi H-8100 TEM and high-resolution TEM (HR-TEM) images were obtained using a JEOL JEM-2100F FEG Fas-TEM. UV-Vis absorption data were obtained using a Cary-5000 UV-Vis spectrophotometer.

Calculated Spectra. DDA calculations were performed on a bipyramid (BP) with an effective edge length of a = 270 nm with b ~ 156 nm and h ~ 89 nm calculated from the equations in Figure 1F. Orientationally-averaged calculations were performed where the BP target was assumed to have two unit vectors $\hat{\mathbf{a}}_1$ and $\hat{\mathbf{a}}_2$ fixed within the target with $\hat{\mathbf{a}}_1$ describing the height (h) (along the x-axis) of the BP and $\hat{\mathbf{a}}_2$ orthogonal to $\hat{\mathbf{a}}_1$. To perform orientation averaging, the BP target was rotated 90° (in three

incremental steps) through the angles of θ and ϕ which specify the direction of $\hat{\mathbf{a}}_1$ with respect to the incident wavevector k. The wavevector was taken to be along the x-axis and polarization along both y- and z-axes was considered. The dielectric table of Frederikse and Weaver[2] for electropolished Au was used and the incident wavelength and the refractive index were divided by the refractive index of water (1.331) to get the relative refractive index. A dipole spacing of 2 nm was used with a spectral resolution of 10 nm.

The normalized calculated BP extinction spectrum (Figure 3B) displays resonance peaks very close to those measured experimentally with UV-Vis spectroscopy with a dipole mode (n = 1) evident at ~1110 nm, a higher order quadrupole mode (n = 2) at ~750 nm, and an octopole mode (n = 3) at ~600 nm. The synthesized BPs have slightly rounded edges and an average size distribution of a = 270 nm ± 26 nm. Neither the rounded edges nor averaging over the size distribution has been considered in the calculated spectrum in Figure 3B. Considering the excellent agreement between calculated and experimental resonant wavelengths this would suggest that there is apparently a cancellation of effects due to edge rounding and size distribution averaging. However averaging over a distribution of edge sizes will broaden and reduce the intensity of the 1110 nm peak in Fig. 3B while not changing the intensity of the 750 nm and 600 nm peaks as higher multipoles are less sensitive to inhomogeneities than is the dipole mode.

Additional calculations (not shown here) with the BP orientation fixed with respect to the incident polarization were performed to provide further insights to the assignment of these modes. The dipole resonance involves polarization that is primarily in the equatorial plane of the BP. The first multipole (n = 2 at ~750 nm) is mostly an in-plane quadrupole, while the octopole (n = 3 at ~600 nm) is a combination of both the in-plane and out-of-plane excitations. There are small shifts between in-plane and out-of-plane extinction maxima for the octopole and as a result the orientationally-averaged spectrum is broad and not entirely symmetrical.

(1) Niu, W. X.; Zheng, S. L.; Wang, D. W.; Liu, X. Q.; Li, H. J.; Han, S. A.; Chen, J.; Tang, Z. Y.; Xu, G. B. *J. Am. Chem. Soc.* **2009**, *131*, 697.
(2) Weaver, J. H.; Frederikse, H. P. R. *Optical properties of selected elements, 82nd ed.* CRC Press: Boca Raton, 2001, p 12.

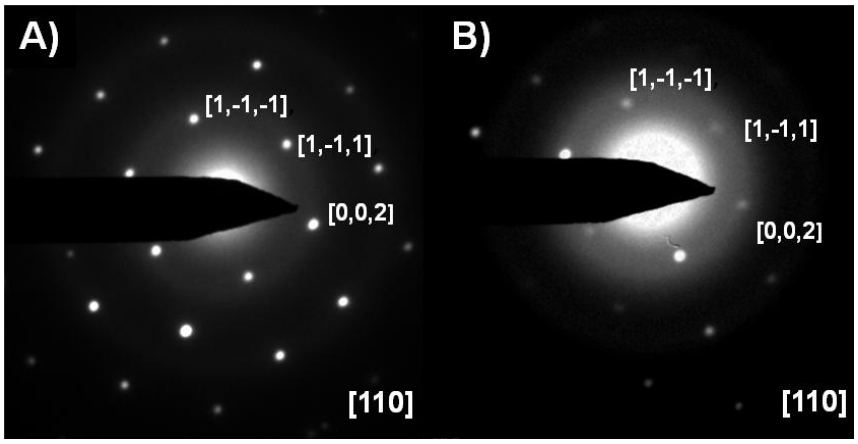

Figure S1. Diffraction patterns of (A) bipyramids and (B) rhombic dodecahedra with {110} facet oriented perpendicular to electron beam.

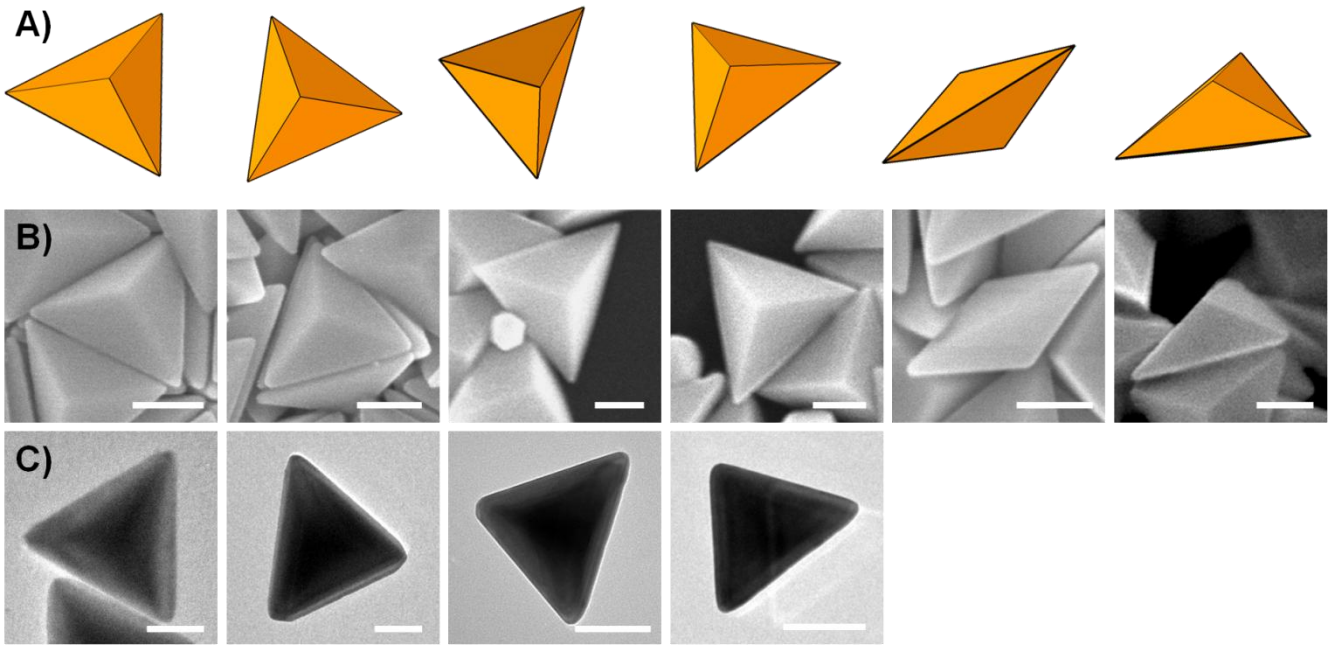

Figure S2. (A) Model, (B) high-magnification SEM, and (C) TEM of individual bipyramids in various orientations. Scale bars: 100 nm.

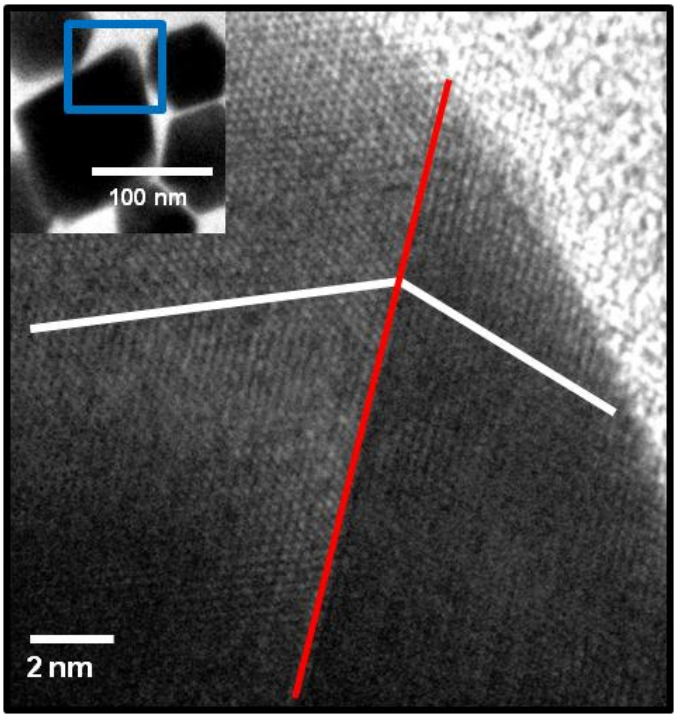

Figure S3. HR-TEM image of a single bipyramid (inset) containing a twin plane (red line).

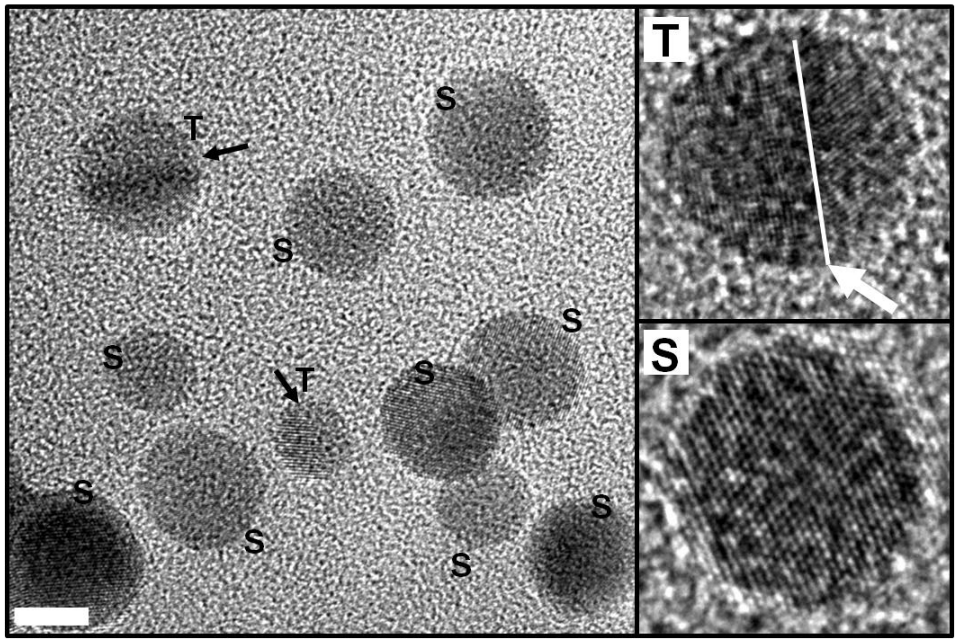

Figure S4. Left: HR-TEM of CTAC-stabilized seed particles. Both twinned and single-crystal seeds are observed, indicated by a T or an S, respectively. Arrows indicate twin boundaries. Scale bar: 5 nm. Right: Examples of twinned (top) and single-crystalline (bottom) seed particles.

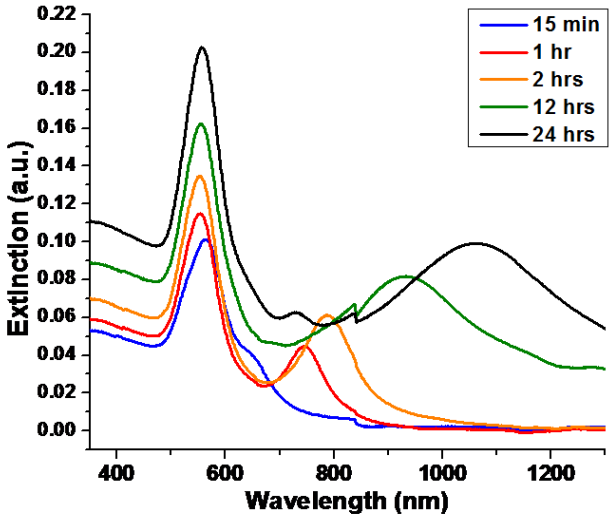

Figure S5. Time-dependent UV-vis spectra monitoring the growth of RD and BPs.

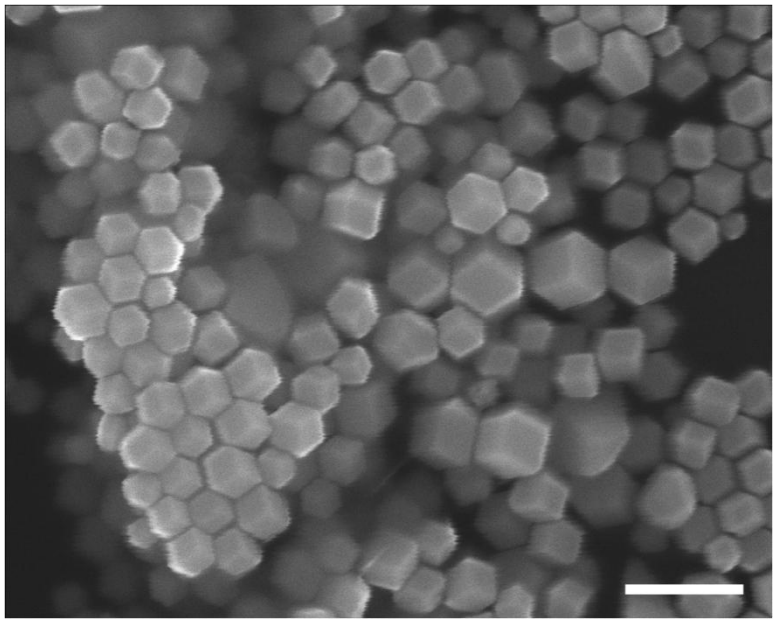

Figure S6. SEM of rhombic dodecahedra synthesized with single-crystal seeds. Scale bar: 200 nm.

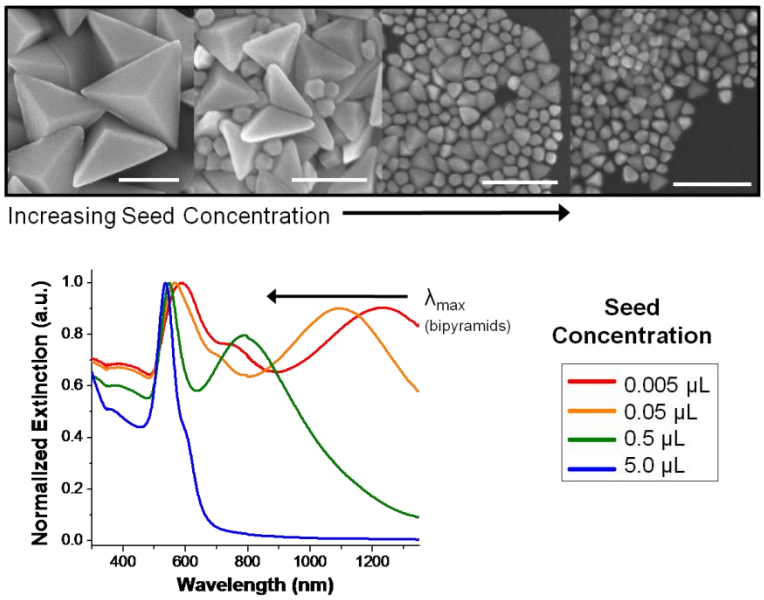

Figure S7. Bipyramids and rhombic dodecahedra grown from the addition of (left to right): 0.005 µL, 0.05 µL, 0.5 µL, and 5.0 µL of seed solution. Scale bars: 200 nm. UV-Vis spectra of RD/BP solutions synthesized from increasing amounts of seed particles. Increasing seed concentration results in smaller product particles.

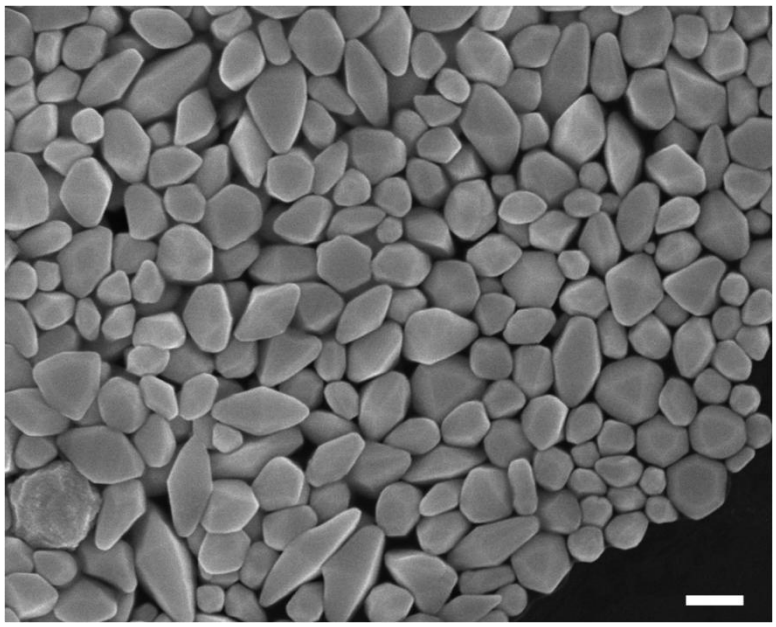

Figure S8. SEM of particles synthesized in CTAB with 10 μM Ag^{+}. Scale bar: 200 nm.